

AD-A261 983



2

RL-TR-92-310  
In-House Report  
December 1992



# MODIFIED ACOUSTO-OPTIC ADAPTIVE PROCESSOR (Mod-AOAP)

Christopher W. Keefer, Captain, USAF; John E. Malowicki;  
Paul M. Payson



*APPROVED FOR PUBLIC RELEASE; DISTRIBUTION UNLIMITED.*

98 3 22 014

93-05919



35 PY

Rome Laboratory  
Air Force Materiel Command  
Griffiss Air Force Base, New York

This report has been reviewed by the Rome Laboratory Public Affairs Office (PA) and is releasable to the National Technical Information Service (NTIS). At NTIS it will be releasable to the general public, including foreign nations.

Although this report references limited documents listed below, no limited information has been extracted:

RADC-TR-86-188, Acousto-Optic Adaptive Processor (AOAP)-Phase II, dated November 1986, Distribution authorized to USGO agencies & private individuals or enterprises eligible to obtain export-controlled technical data IAW DODD 5230.25; Nov 86. Other requests must be referred to RL (OCTS), 26 Electronics Parkway, Griffiss AFB NY 13441-4514.

RL-TR-92-13, Acousto-Optic Adaptive Processor (AOAP) Enhancements, dated February 1992, Distribution authorized to USGO agencies & private individuals or enterprises eligible to obtain export-controlled technical data IAW DODD 5230.25; Feb 92. Other requests must be referred to RL (C3DB), 525 Brooks Road, Griffiss AFB NY 13441-4505.

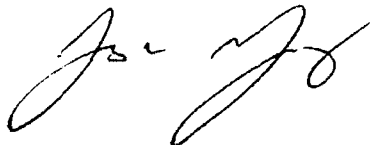
RL-TR-92-310 has been reviewed and is approved for publication.

APPROVED:



JAMES W. CUSACK, Chief  
Photonics and Optics Division  
Surveillance and Photonics Directorate

FOR THE COMMANDER:



JAMES W. YOUNGBERG, Lt Col, USAF  
Deputy Director  
Surveillance and Photonics Directorate

If your address has changed or if you wish to be removed from the Rome Laboratory mailing list, or if the addressee is no longer employed by your organization, please notify RL(OCP ) Griffiss AFB, NY 13441-4515 This will assist us in maintaining a current mailing list.

Do not return copies of this report unless contractual obligations or notices on a specific document require that it be returned.

# REPORT DOCUMENTATION PAGE

Form Approved  
OMB No. 0704-0188

Public reporting burden for this collection of information is estimated to average 1 hour per response, including the time for reviewing instructions, searching existing data sources, gathering and maintaining the data needed, and completing and reviewing the collection of information. Send comments regarding this burden estimate or any other aspect of this collection of information, including suggestions for reducing this burden, to Washington Headquarters Services, Directorate for Information Operations and Reports, 1215 Jefferson Davis Highway, Suite 1204, Arlington, VA 22202-4302, and to the Office of Management and Budget, Paperwork Reduction Project (0704-0188), Washington, DC 20503.

1. AGENCY USE ONLY (Leave Blank)		2. REPORT DATE December 1992		3. REPORT TYPE AND DATES COVERED Final Feb 89 - Jun 92	
4. TITLE AND SUBTITLE MODIFIED ACOUSTO-OPTIC ADAPTIVE PROCESSOR (Mod-AOAP)				5. FUNDING NUMBERS PE - 62702F PR - 4600 TA - P1 WU - 05	
6. AUTHOR(S) Capt Christopher W. Keefer, John E. Malowicki, Paul M. Payson					
7. PERFORMING ORGANIZATION NAME(S) AND ADDRESS(ES) Rome Laboratory (OCP) 25 Electronic Parkway Griffiss AFB NY 13441-4515				8. PERFORMING ORGANIZATION REPORT NUMBER RL-TR-92-310	
9. SPONSORING/MONITORING AGENCY NAME(S) AND ADDRESS(ES) Rome Laboratory (OCP) 25 Electronic Parkway Griffiss AFB NY 13441-4515				10. SPONSORING/MONITORING AGENCY REPORT NUMBER	
11. SUPPLEMENTARY NOTES Rome Laboratory Project Engineer: Capt Christopher W. Keefer/OCPA/(315)330-2944					
12a. DISTRIBUTION/AVAILABILITY STATEMENT Approved for public release; distribution unlimited				12b. DISTRIBUTION CODE	
13. ABSTRACT (Maximum 200 words) Multipath jamming noise introduced into a radar antenna's sidelobes effectively reduces the radar's target detection capability. The acousto-optic adaptive processor (AOAP) was developed to demonstrate an optical implementation of the least mean square (LMS) algorithm for adaptively cancelling noise jamming. The AOAP system demonstrated 30 dB cancellation of monotone CW signals, with degraded performance as the bandwidth increased. The liquid crystal light valve (LCLV), used as the integrator/spatial light modulator in the AOAP, has been identified as limiting system performance. In this report we report on modifications to the AOAP. Specifically, the LCLV has been replaced with a photorefractive crystal. Cancellation performance and cancellation speed of the mod-AOAP are presented and compared to the original results.					
14. SUBJECT TERMS Adaptive Processing, Acousto-Optics, Optical Signal Processing, Photorefractive Devices				15. NUMBER OF PAGES 40	
				16. PRICE CODE	
17. SECURITY CLASSIFICATION OF REPORT UNCLASSIFIED		18. SECURITY CLASSIFICATION OF THIS PAGE UNCLASSIFIED		19. SECURITY CLASSIFICATION OF ABSTRACT UNCLASSIFIED	
				20. LIMITATION OF ABSTRACT UL	

## Table of Contents

	<u>Pg</u>
List of Figures	v
Acknowledgements	vi
1. Introduction	1
1.1 Background	1
1.2 Purpose	1
1.3 Approach	1
1.4 Organization of Report	1
2. Adaptive Optical Processor Concept	2
2.1 General Scenario	2
2.2 Adaptive Noise Cancelling Concept	3
2.3 Multipath Jamming Cancellation	4
2.3.1 Acousto-Optic Delay Line	5
2.3.2 Optical Integrator/Spatial Light Modulator	6
2.3.2.1 Liquid Crystal Light Valve	6
2.3.2.2 Photorefractive Crystal	7
2.4 AOAP Optical Layout	8
2.4.1 Time Integrating Correlator	8
2.4.2 Space Integrating Correlator	8
2.5 AOAP Performance	9
3. Modified AOAP and Experimental Results	9
3.1 Time Integrating Correlator	10
3.2 Space Integrating Correlator	11
3.3 Signal Simulation Hardware	11
3.4 Experimental Results	13
3.4.1 Cancellation with Applied DC Field	13
3.4.2 Cancellation with Applied AC Field	15
3.4.3 Cancellation Speed	17

4. Discussion	Pg 17
4.1 Predicted Cancellation	18
4.2 Comparison of AOAP and mod-AOAP	20
5. Conclusions and Recommendations	20
5.1 Conclusions	20
5.2 Recommendations	20
References	21
Appendix - Diffraction efficiency simulation program	23

<b>Accession For</b>	
NTIS GRA&I	<input checked="" type="checkbox"/>
DTIC TAB	<input type="checkbox"/>
Unannounced	<input type="checkbox"/>
Justification	
By _____	
Distribution/	
<b>Availability Codes</b>	
<b>Dist</b>	<b>Avail and/or Special</b>
A-1	

## List of Figures

	<u>Pg</u>
1. General scenario for sidelobe jamming.	2
2. Block diagram of LMS algorithm.	4
3. Diagram of acousto-optic cell demonstrating variable delay.	5
4. Measured MTF as a function of grating period for the LCLV supplied with the AOAP.	7
5. Original AOAP optical layout.	9
6. Opto-electronic layout of mod-AOAP incorporating BSO crystal.	10
7. Expanded view of mod-AOAP time integrating correlator subsystem.	11
8. Expanded view of mod-AOAP space integrating correlator subsystem.	12
9. Cancellation of 40-MHz monotone CW signal with applied DC field.	13
10. Cancellation of wideband noise signals a) 100, b) 200, and c) 500 kHz centered at 40 MHz with applied DC field.	14
11. Cancellation of 40-MHz monotone CW signal with applied AC field.	15
12. Cancellation of wideband noise signals a) 100, b) 200, and c) 500 kHz centered at 40 MHz with applied AC field.	16
13. Cancellation of 40-MHz monotone CW signal with respect to time.	17
14. Block diagram of mod-AOAP closed loop system gain components.	18
15. Predicted diffraction efficiency versus noise signal bandwidth.	19
16. Normalized system gain with respect to noise signal bandwidth.	19

## **Acknowledgements**

The fabrication and testing of the mod-AOAP has been performed in-house at the Rome Laboratory Photonics Center. The authors wish to acknowledge the help of several scientists and engineers who provided assistance during this project: Fred Vachss and John Hong of Rockwell International Science Center, who assisted in the design of the mod-AOAP using the photorefractive crystal; George Brost of RL/OCPA, who provided many insights into the characteristics of the BSO crystal and its operation in the adaptive processor; Bob Iodice of General Electric who helped troubleshoot the signal simulation hardware; and the many other in-house personnel who supported this effort.

## 1. Introduction

**1.1 Background.** A desirable function of radar signal processing is to eradicate jamming noise from the radar return. Jamming noise introduced into a radar antenna's sidelobes effectively reduces the radar's target detection capability. Electronic sidelobe cancelers have been developed as a countermeasure to sidelobe jamming, however, performance is limited when the radar operates in a multipath jamming environment. An optical processing approach exploits the potential of acousto-optic (AO) cells to process a continuum of multipath delays in parallel. The use of an optical integrator suppresses the need to perform analog to digital conversion which is a time consuming task. There have been a number of papers reporting on the performance of optical adaptive signal processors.<sup>1,2,3,4,5</sup>

**1.2 Purpose.** The purpose of this effort was to evaluate and improve upon the design of the Acousto-Optic Adaptive Processor (AOAP) developed by General Electric under RADC contract numbers F30602-81-C-0264 and F30602-88-C-0141.<sup>1,2</sup> The AOAP concept was designed to cancel radar interference, such as external jamming, while passing desired signals such as radar echoes onto the radar's signal processor. The figures of merit for evaluating the AOAP are the ability to cancel CW and wideband jamming signals and the cancellation speed.

**1.3 Approach.** General Electric delivered the AOAP to Rome Laboratory in September 1990 for evaluation and enhancement. General Electric identified the liquid crystal light valve (LCLV) as limiting the AOAP's performance.<sup>2</sup> The first phase of our effort was to measure the LCLV performance. The 1985 Hughes LCLV performance has deteriorated greatly over the years. The LCLV was unable to perform the desired integration function in the AOAP. The second phase of the effort was to enhance the AOAP by replacing the LCLV. A  $Bi_{12}SiO_{20}$  (BSO) photorefractive crystal (PRC) was chosen as the replacement for the LCLV. This particular type of crystal was chosen because of its response time (on the order of msec's), visible wavelength (400-700 nm) operation, and large dynamic range (> 40 dB)<sup>4</sup>. In this report we compare the performance of the AOAP configuration using the PRC with the results obtained by GE using the LCLV. The results obtained with the PRC do not significantly improve upon the GE results in terms of cancellation ratio. However, the device performs the cancellation in approximately 1 msec which is an improvement upon the LCLV based adaptive processor.

**1.4 Organization of Report.** Section 2 of this report provides an overview of multiple sidelobe cancellation using an optical processor. This section includes a description of the AOAP and its measured performance. Section 3 describes the modified optical implementation of the AOAP incorporating the PRC. A detailed description of the time integrating and space integrating correlator architectures is presented along with test results using the PRC. The mod-AOAPs results are analyzed in Section 4. Conclusions and recommendations for further study are presented in Section 5.



## 2. Adaptive Optical Processor Concept

**2.1 General Scenario.** Fig. 1 depicts the scenario of a hypothetical ground-based radar system facing electronic countermeasure threats of noise jamming incident on the sidelobes.

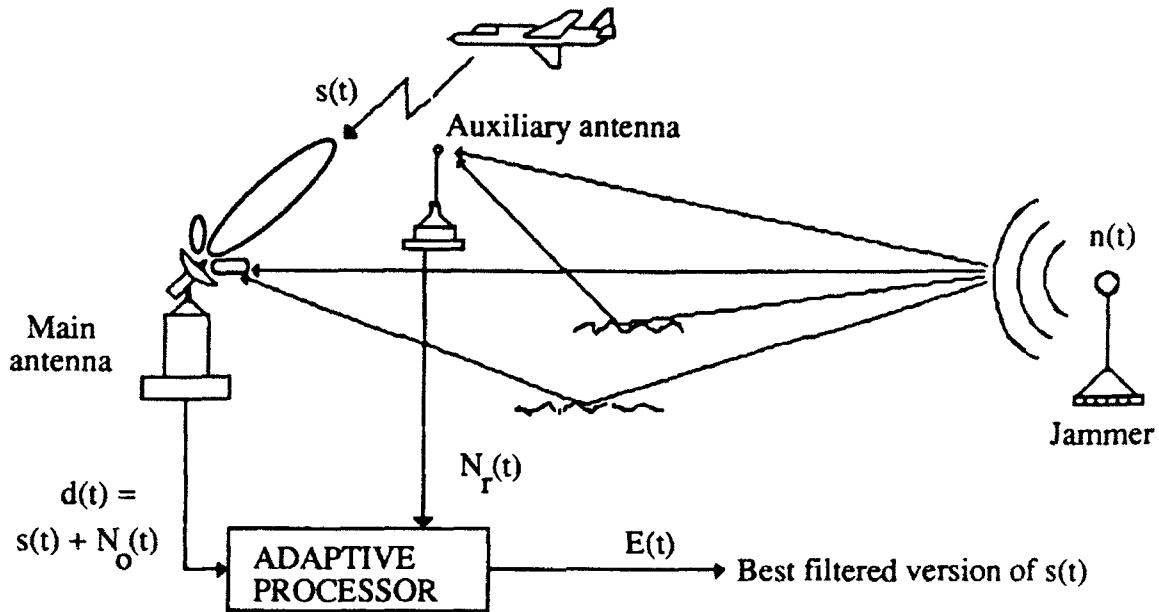


Fig.1 General scenario for sidelobe jamming.

In this figure the jamming source  $n(t)$ , which contains frequencies in the radar's passband, enters through the radar's sidelobes. The main antenna receives the signal

$$d(t) = s(t) + N_o(t) \quad (1)$$

where  $s(t)$  is the target return and  $N_o(t)$  is the jammer noise received in the main antenna. The received jammer noise is expressed as a multiple delayed version of the jammer source

$$N_o(t) = \sum_{m=1}^M A_{om} n(t - \tau_{om}) \quad (2)$$

where  $M$  is the number of multipath reflections,  $A_{om}$  is the received gain of the  $m$ th multipath and  $\tau_{om}$  is the time delay of the  $m$ th multipath of noise source  $n(t)$ .

The auxiliary antenna in Fig. 1 receives the signal

$$N_r(t) = \sum_{m=1}^M A_{r_m} n(t-\tau_{r_m}) \quad (3)$$

where  $A_{r_m}$  is the received gain of the  $m$ th multipath and  $\tau_{r_m}$  is the time delay of the  $m$ th multipath of noise source  $n(t)$ . The direct path interference is for  $m = 1$ .

**2.2 Adaptive Noise Canceling Concept.** Howells and Applebaum developed a technique called the intermediate frequency (IF) sidelobe canceler to counter the jamming threat.<sup>6</sup> This technique senses the jamming environment with an omnidirectional auxiliary antenna, adaptively weights the auxiliary signal in amplitude and phase, and subtracts it from the main radar channel. The adaptive weighting process consists of cross-correlating the radar signal with the noise signals received by the auxiliary antenna to determine the amplitude and phase of the offending interference and subtract this precise signal from the radar signal. The net effect is to reduce the main antenna's sidelobe gain in the direction of the jammer through adaptive noise canceling.

If the characteristics of the jamming signal are known it would be possible to design a fixed filter to subtract out the noise in the radar signal. However, because the transmission paths of the jamming signal are unknown and seldom fixed, an adaptive filter which automatically adjusts its impulse response is necessary. The least mean square (LMS) algorithm is widely used for adaptive filtering. Reference 7 provides a detailed description of the LMS algorithm. A block diagram of the implementation is shown in Fig. 2.

The auxiliary antenna's output signal  $N_r(t)$  is the reference input to the adaptive algorithm in Fig. 2. The other input  $E(t)$ , see Eq. 6, consists of the algorithm's output  $y(t)$ , see Eq. 5, subtracted from the radar antenna's output  $d(t)$ . The jamming noise signal  $N_r(t)$  is uncorrelated with the radar signal  $s(t)$  and correlated in an unknown way with the jamming noise signal  $N_o(t)$ . The algorithm finds the correlation between  $E(t)$  and  $N_r(t)$  by multiplication of the inputs and integration of the result. The correlation result is referred to as the correlation weight vector  $w(\tau)$

$$w(\tau) = \int_0^{T_{int}} E(t) N_r^*(t - \tau) dt \quad (4)$$

where  $T_{int}$  is the integration time and  $\tau$  is the multipath time delay variable. This weight vector is

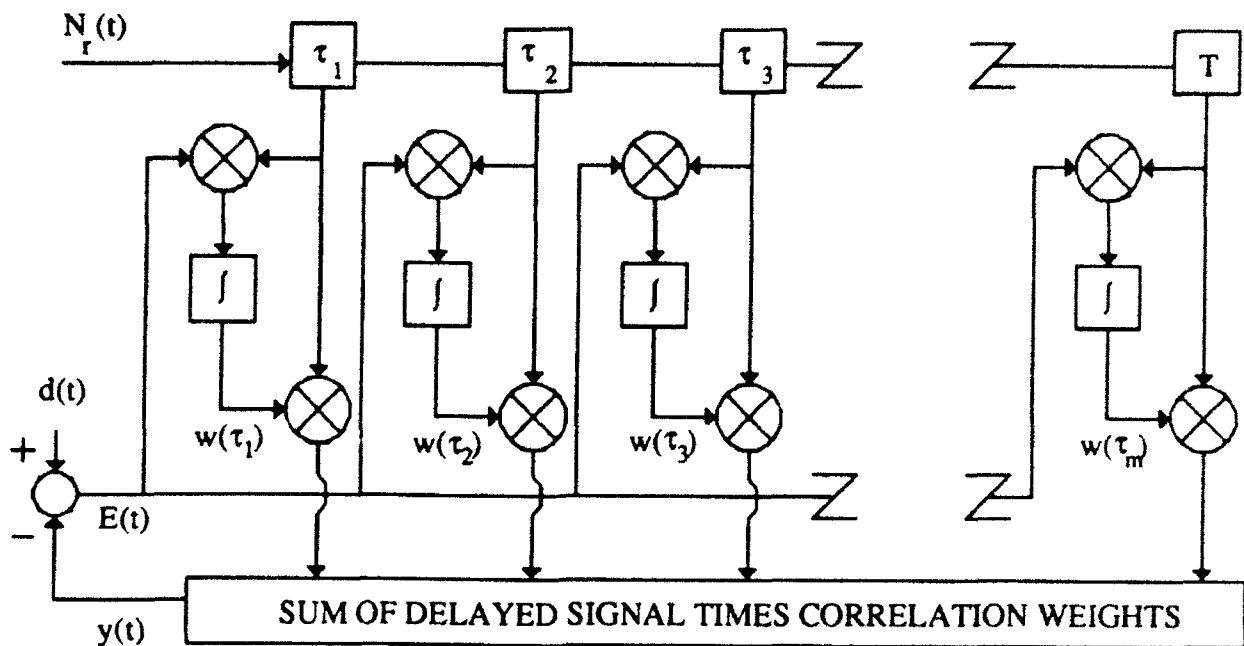


Fig. 2. Block diagram of LMS algorithm.

then convolved with the reference signal  $N_r(t)$  by a multiplication to form a weighted version of the noise

$$y(t) = \int_0^T w(\tau) N_r(t - \tau) dt \quad (5)$$

where  $T$  is the temporal length of the delay line. The noise estimate  $y(t)$  is subtracted from the radar input  $d(t)$  to produce the error function

$$E(t) = d(t) - y(t) \quad (6)$$

The result is again correlated with the noise  $N_r(t)$  and the process is repeated. The expected value of  $E(t)$  is shown to approach a minimum without effecting the signal of interest  $s(t)$ <sup>7</sup>. If the noise environment changes the algorithm will adapt to filter out the new noise characteristics.

**2.3 Multipath Jamming Cancellation.** The series of delays  $\tau$  across the top of the block diagram of Fig. 2 represent the large number of possible delays generated in the multipath environment. For a real time processing system the multiplication and integration for each delay needs to be accomplished in parallel. Also, the convolution and summing of the noise estimates

for each delay need to be accomplished in parallel. An optical implementation exploits the inherent parallelism of optical processing to efficiently implement the multipath LMS algorithm. The correlation of the main and reference signal is performed by an optical time integrating correlator. The summing of the noise estimates for each delay is performed by an optical space integrating correlator. The two key optical technologies for implementing the time and space integrating correlators in parallel are the AO delay line and an integrator/spatial light modulator (SLM).

**2.3.1 Acousto-Optic Delay Line.** The acousto-optic (AO) cell forms the interface between the electrical and optical systems for implementing the LMS algorithm. A diagram of the AO cell is shown in Fig 3.

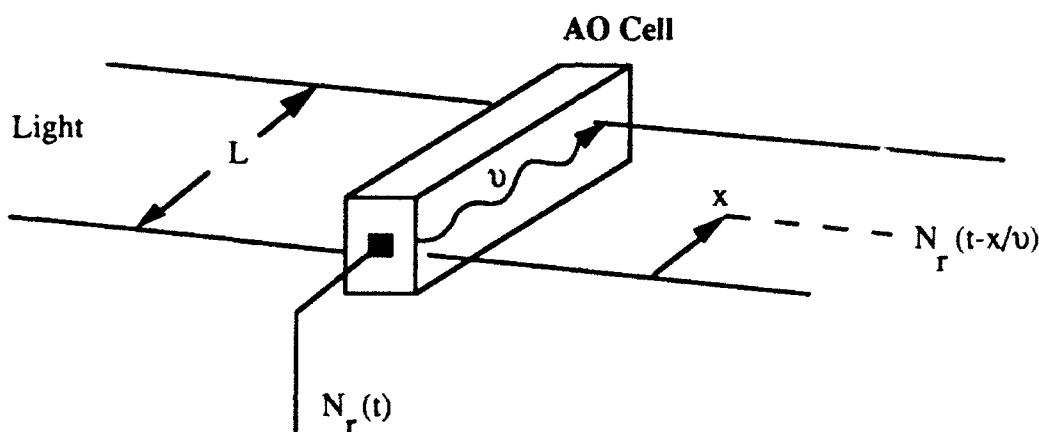


Fig. 3. Diagram of acousto-optic cell demonstrating variable delay.

A transducer attached to one end of the AO cell launches an acoustic wave proportional to the signal input  $N_r(t)$ . If  $v$  is the acoustic velocity in the AO cell material and  $x$  is the distance traveled from the transducer, then  $\tau = x/v$  is the time delay to any position in the AO cell. An AO cell, with time aperture of length  $L$ , can be used to process all possible delays between 0 and  $T = L/v$  simultaneously. The AO cell is inherently suited to represent the multiple delays in the LMS algorithm. If an RF signal  $n(t - \tau_{rm}) = \cos 2\pi f_c(t - \tau_{rm})$ , where  $f_c$  is the carrier frequency of the AO cell, is applied to the transducer of the AO cell and the AO cell is illuminated with a uniform beam of light across its aperture, the light will be diffracted at an angle proportional to the frequency  $f_c$  applied to the AO cell.<sup>8</sup> The interference between the partially depleted incident wave and the diffracted wave from the AO cell produces a traveling wave at the image plane of the AO cell that has an optical intensity pattern

$$I(x,t) = I_0(t)[1 + 2\sqrt{\eta_1(1-\eta_1)} \sin 2\pi f_c(t - \tau_{rm} - x/v)] \quad (7)$$

which is a replica of the acoustic wave, where  $I_0(t)$  is the incident illuminating intensity and  $\eta_1$  is

the diffraction efficiency of the AO cell. If the light source is modulated at the same frequency as those terms in the traveling wave pattern

$$I_0(t) = I_0[1 + m_s \cos 2\pi f_c(t - \tau_{om})], \quad (8)$$

where  $I_0$  is the light source intensity and  $m_s$  is the fractional modulation of the source intensity, then a stationary fringe pattern is produced in the image plane of the AO cell. If the input to the AO cell is  $N_r(t)$  and the laser is modulated with  $E(t)$ , then the stationary fringe pattern corresponds to the multiplication of  $E(t)$  and  $N_r(t)$  in Fig. 2. A time integrating device placed in the image plane of the AO cell will capture the integrated exposure corresponding to the correlation between  $E(t)$  and  $N_r(t)$ .

**2.3.2 Optical Integrator/Spatial Light Modulator.** The integrated exposure function is represented as

$$I(x,t) = I_0[1 - m_s \sqrt{\eta_1(1-\eta_1)} \sin 2\pi f_c(\tau_{om} - \tau_{rm} - x/v)] \quad (9)$$

A charged coupled device (CCD) array could be used to perform the integration. However, the output of the CCD array must be transferred to a spatial light modulating device to perform the convolution with  $n(t)$  in the space integrating correlator described in Section 2. The CCD array is also a pixellated device which means there is a limit to the delay resolution in Eq. 9. An alternate approach is to use an optically addressed SLM which performs a linear time integrating function. Two such devices are the LCLV and the PRC.

**2.3.2.1 Liquid Crystal Light Valve.** The LCLV provides the necessary square law detection of the input correlation and then is able to spatially modulate an optically coherent carrier with this information. Reference 9 provides a detailed description of the LCLV. The device consists of two sections, which are optically isolated, to form the integrator/ spatial light modulator pair. The "writing" light falls on a CdS photoconductive layer. This layer interacts with an AC bias voltage to produce an electrical field across the liquid crystal in the second section. The electric field's spatial pattern is an image of the incident light pattern. Coherent "read" light is transmitted through the liquid crystal layer and reflected by a dichroic mirror back through the liquid crystal layer. The electric field in the liquid crystal layer causes the light to change polarization as it passes through the liquid crystal. The use of a polarizer/analyzer pair before and after the LCLV is necessary to generate the spatial amplitude modulation of the light with the LCLV.

Tests of the LCLV delivered with the AOAP revealed the performance has degraded over the years. Fig. 4 shows the measured modulation transfer function (MTF) of the LCLV with respect to different grating frequencies which were imaged onto the write side of the device. The AOAP requires a resolution of greater than 10 lines/mm to function properly. A MTF of at least 0.5 at 10 l/mm is needed to achieve high contrast in the grating formed at the LCLV. Mr Paul Ruterbusch of GE<sup>10</sup> measured the LCLV's MTF at 10 lines/mm to be 0.01, which makes the

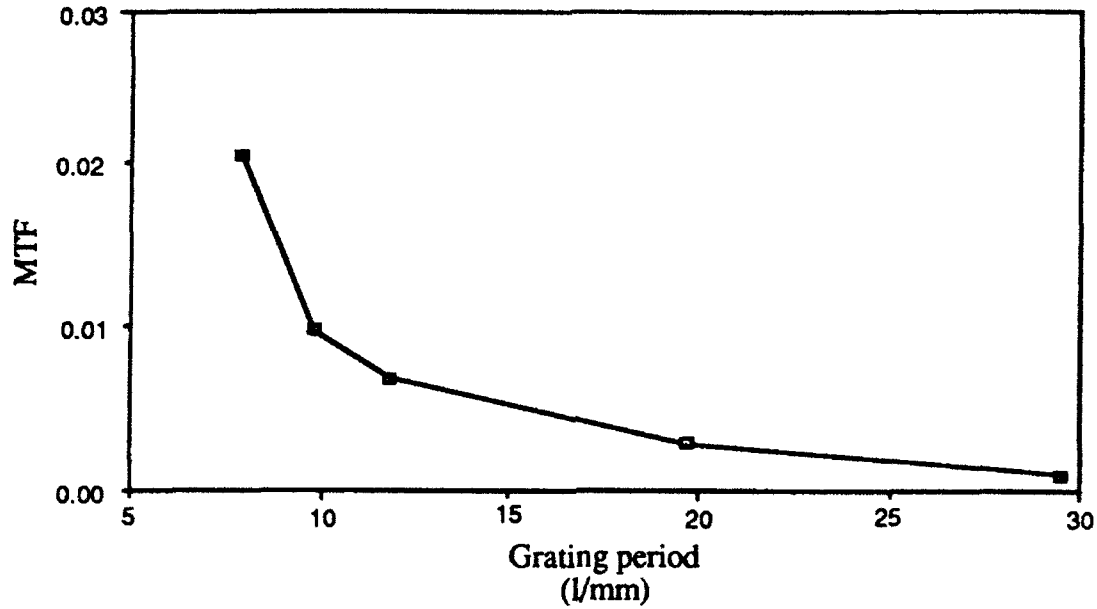


Fig. 4. Measured MTF as a function of grating period for the LCLV supplied with the AOAP.

device useless for this application. An alternate optical integrator/spatial light modulator is the photorefractive crystal.

**2.3.2.2 Photorefractive Crystal.** The PRC provides the ability to perform a square law detection of the input intensity pattern and spatially modulate a "read" light source with this information. The holographic grating recording technique in photorefractive crystals is based on photo-induced changes in the refractive index of the electro-optic material. In this process, electrons are excited from traps in regions of high optical intensity. The electrons move to regions of low optical intensity where recombination occurs. The recombination generates a spatially varying space-charge field. Through the linear electro-optic effect a corresponding modulation of the refractive index profile is present in the photorefractive crystal. These effects have been reported on quite thoroughly.<sup>11</sup> For purposes of this report the photorefractive model is simplified to highlight the main features of the photorefractive based correlator. The PRC can be used as the time integrating device in the image plane of the AO cell to record the stationary fringe pattern as a space charge field. The space charge field is represented as

$$E_{sc} = -m_s E_0 [\eta_1 (1 - \eta_1) \sin 2\pi f_c (\tau_{om} + \tau_{rm} + x/v)] \quad (10)$$

where  $E_0$  is the strength of the applied bias field. The refractive index variation is proportional to this space charge field and the grating diffraction efficiency  $\eta_2$  is proportional to the space charge field squared.<sup>8</sup> The second function performed by the photorefractive element is that the grating formed in the crystal can be read out and multiplied with the moving acoustic signal (also

proportional to  $N_r(t)$ ) transversing a second AO cell. The product of the correlation weight vector  $w(\tau)$  from the photorefractive crystal and the acoustic signal on the second AO cell consists of detecting the heterodyne beat between the frequency shifted light diffracted by the AO cell and the unshifted light diffracted by the stationary grating in the photorefractive element. The multiplication is accomplished by imaging the PRC's stationary grating into the Bragg cell. A Fourier lens after the AO cell sums the continuum of delays across the AO cell to a common point where a photodiode is placed. This part of the optical system is the space integrating correlator discussed in Section 2.1

**2.4 AOAP Layout.** The optical layout of the original AOAP design is shown in Fig. 5. A detailed description of this system is presented in Reference 5. An electronic subtraction system is used to close the AOAP adaptive loop after the detector output. There are a number of electronic amplifiers and mixers necessary to drive the AO modulator and delay lines. This section will focus on the optical system. The beam from a CW Argon-ion laser is split into two paths by a beamsplitter. This is necessary to perform the two operations of the time integrating correlator and space integrating correlator.

**2.4.1 Time Integrating Correlator.** The transmitted beam from the first beamsplitter cube after the laser is focused into an AO modulator, which amplitude modulates the laser with the main channel residue signal,  $E(t)$ . In order to achieve amplitude modulation the beam must be focused smaller than one wavelength of the carrier frequency of the AO modulator. The diffracted order from the AO modulator contains the modulated beam. This beam is spatially filtered and collimated before being used to illuminate the first reference AO delay line which has a RF input  $N_r(t)$ . The AO delay line is imaged with a two lens imaging system onto the input side of the LCLV. The LCLV responds to the incident light pattern by spatially modulating the readout beam on its opposite side.

**2.4.2 Space Integrating Correlator.** The reflected beam from the first beamsplitter cube after the laser is used for the space integrating correlator subsystem of the AOAP. The laser light is spatially filtered and collimated in the same exact manner as the laser light in the time integrating correlator. The expanded laser light passes through a polarizer and reflects off a second beamsplitter cube into the liquid crystal layer of the LCLV. The resulting spatially modulated beam is reflected back through the beamsplitter cube. The transmitted light through the beamsplitter passes through another polarizer. The two polarizers provide the polarizer/analyzer pair necessary for optimum diffraction performance of the LCLV. The resulting spatial modulation is imaged onto a second AO delay line which carries the same reference signal  $N_r(t)$  as the first AO delay line. The two lens imaging system is exactly the same as in the time integrating correlator. The resulting product in the second AO delay line is collected by the final lens and interferes at the detector. The detected signal is amplified and electronically subtracted from the main channel signal residue signal  $E(t)$  to close the loop.

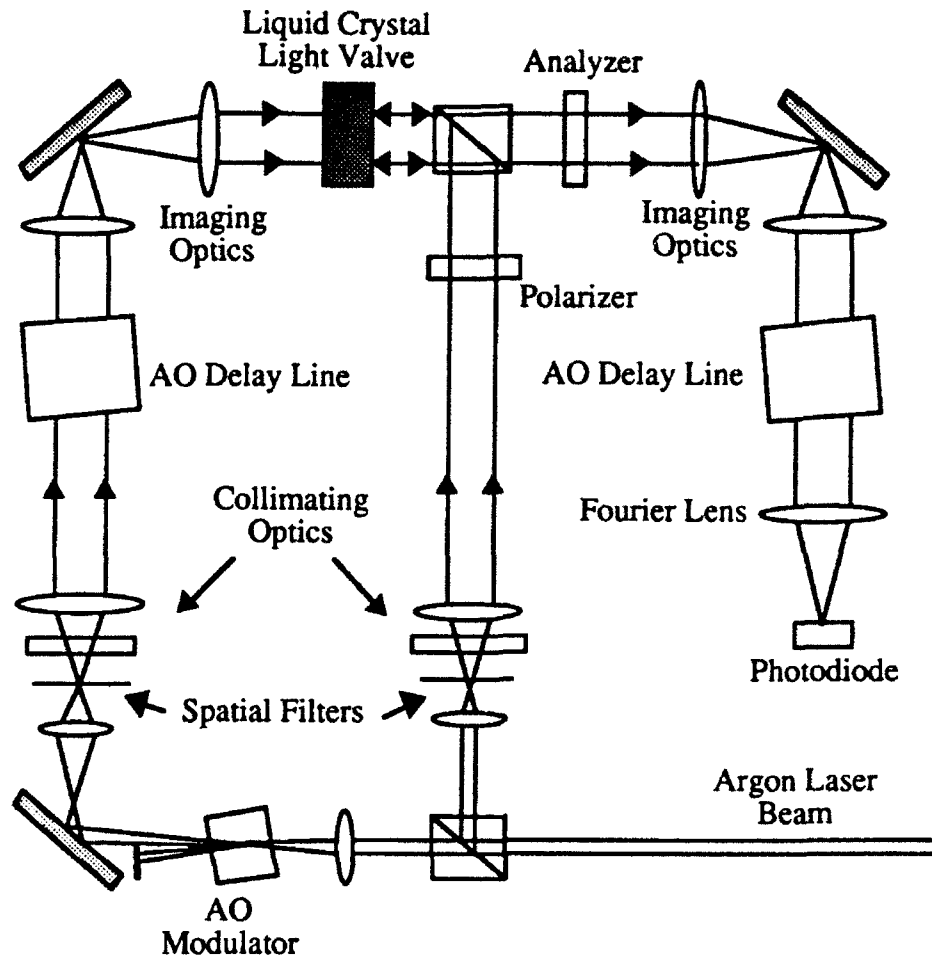


Fig. 5. Original AOAP layout.

**2.5 AOAP Performance.** The AOAP was not tested in-house because the LCLV was not in working order. The following results are those provided by GE in Reference 2. The AOAP provides approximately 30-dB cancellation of monotone CW signals, approximately 20-dB cancellation of a 10-kHz bandwidth signal centered at 40 MHz, and 15-dB cancellation of a 1-MHz bandwidth signal centered at 40 MHz. The cancellation speed of the AOAP was not measured<sup>2</sup>, however, the response of the LCLV is approximately 20 msec which provides a good estimate of the cancellation speed of the AOAP. These results are presented for comparison to the performance of the mod-AOAP presented in Section 3.

### 3. Modified AOAP and Experimental Results

Minor modifications were made to the original AOAP architecture to replace the LCLV with the BSO crystal. The opto-electronic implementation is detailed in Fig. 6.



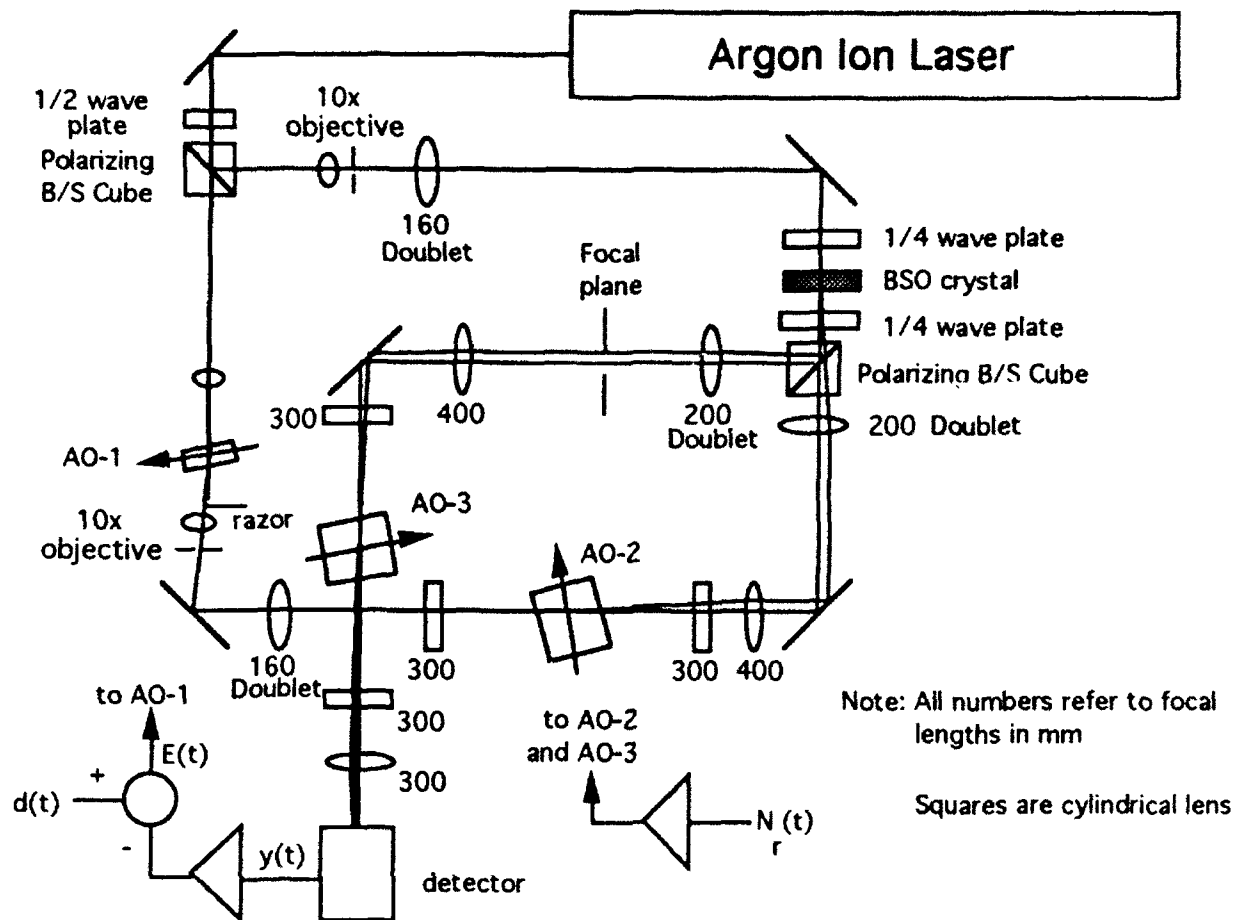


Fig. 6. Opto-electronic layout of the mod-AOAP incorporating the BSO crystal .

**3.1 Time Integrating Correlator.** An argon-ion laser is used as the light source for both the time integrating and space-integrating correlators. The time integrating correlator subsystem begins with the laser beam focused into an Isomet Model 1250C AO modulator, AO-1. This cell is driven by an external RF signal containing  $E(t) = d(t) - y(t)$  modulating a 200-MHz carrier. The cell is used to intensity modulate the laser beam with  $E(t)$ . An expanded view of the time integrating correlator in the mod-AOAP is shown in Fig. 7. The temporally modulated beam is then spatially filtered and sent into an IntraAction AOD-40 deflector cell, AO-2, driven by another RF signal  $N_r(t)$  which represents the jamming noise collected by the auxiliary antenna. The output of AO-2 is imaged and demagnified onto the PRC as shown. Demagnification is used because the BSO crystal is 1 cm in width compared to the 2-cm width of the AO cell. The quarter wave plate used before and after the PRC ensures circularly polarized light enters the PRC to improve overall diffraction efficiency. The BSO crystal is biased with an electric field  $E_0$  in the 110 direction to improve diffraction efficiency. Experimental results are presented for 1) an applied bias of 8 kV DC and 2) an applied bias of a 4 kV p-p, 1.6 kHz AC square wave.

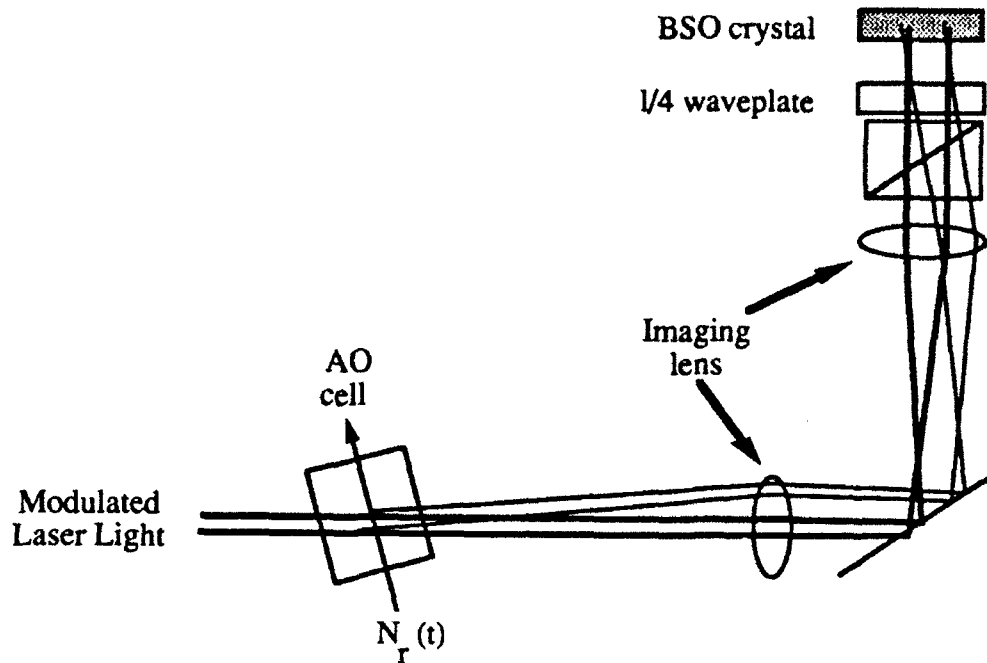


Fig. 7. Expanded view of mod-ACAP time integrating correlator subsystem.

**3.2 Space Integrating Correlator.** The space integrating correlator subsystem requires using the unmodulated portion of the laser beam to image the correlation results of the PRC onto another IntraAction AOD-40 deflector cell, AO-3, which also contains  $N_r(t)$ . The telescope configuration magnifies the image to fill the input window of AO-3. As can be seen in Fig. 8, the diffracted order from the AO cell overlaps a diffracted order from the PRC and these are collected onto the detector where heterodyning occurs. The detector output should consist of a properly weighted delayed version of  $N_r(t)$  corresponding to the noise  $N_o(t)$  in  $d(t)$ . The detector output  $y(t)$  is amplified and subtracted from  $d(t)$  resulting in the cancellation of the jamming signal. The resulting signal  $E(t)$  is again used to drive AO-1 which closes the adaptive loop. In our system tests, the signals for  $d(t)$  and  $N_r(t)$  are the same and generated by the hardware described in the following paragraphs.

**3.3 Signal Simulation Hardware.** The hardware for simulating the noise signals was developed by General Electric to generate correlated broadband signals for both main and auxiliary channels.<sup>2</sup> Its specifications include a high degree of channel to channel amplitude and phase match across a 3-MHz wide bandwidth centered at 40 MHz. With identical broadband digital samples in the main and auxiliary channels, subtraction of the auxiliary output from the main output produces a residue signal at least 50 dB below the main channel output. This degree of channel to channel match ensures that the signal simulator hardware does not interfere with the performance measurements of the optical adaptive processor.<sup>2</sup>

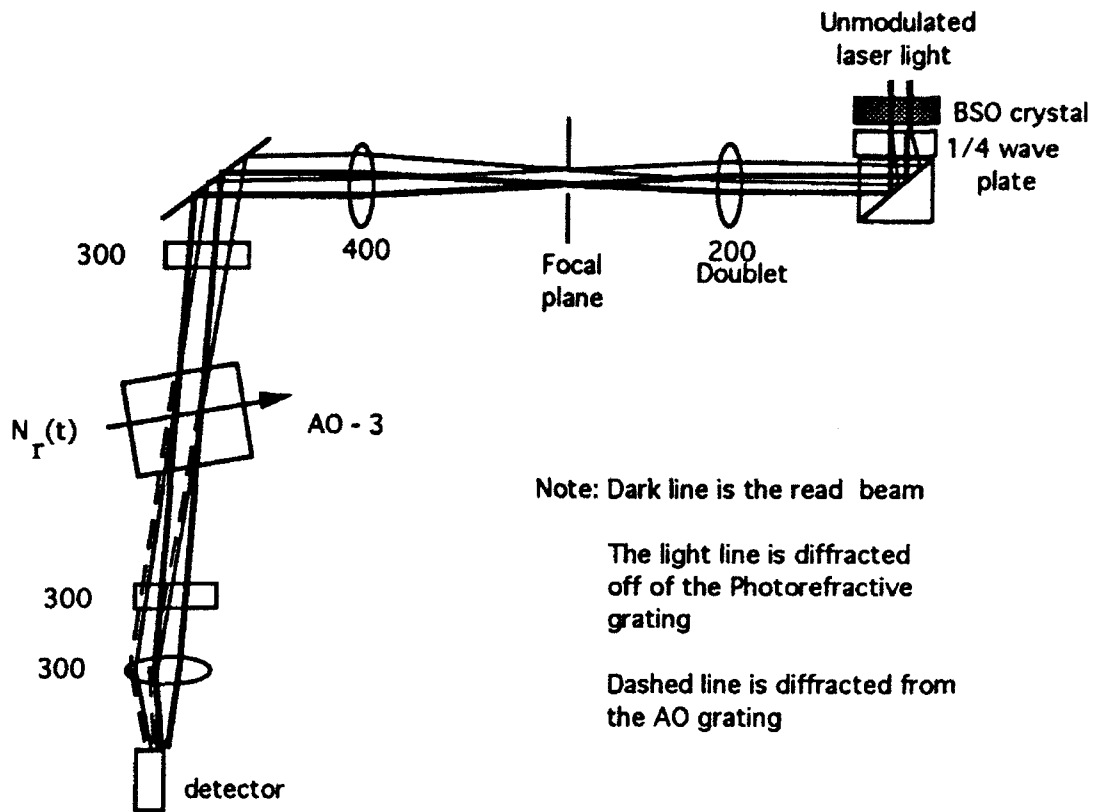


Fig. 8. Expanded view of mod-AOAP space integrating correlator subsystem.

To achieve the specified channel to channel match, digital processing for signal generation is used, delaying the conversion to analog as long as possible. A computer generates the digital signals (either narrow or wideband) of the form

$$n(t) = \sum_{i=1}^I G \cdot \sin[(2\pi f_i t + \tau) + \phi] \quad (11)$$

where  $G$  is a gain factor,  $I$  is the number of different frequencies  $f_i$ ,  $\tau$  is a time delay, and  $\phi$  is a phase shift specified to create the desired signal. As illustrated in Eq. 11, wideband signals are generated by summing multiple sine waves having different frequencies. Both the main and auxiliary channel signals are constructed in this fashion.

The main channel digital signal is buffered in memory, then read out and piped into a D/A conversion board. Once converted to analog, the signal is low pass filtered (22-MHz cutoff) and mixed with a 50-MHz carrier to generate the desired frequency. The mixed output is sent into a

10-MHz wide bandpass filter (BPF) centered at 40 MHz. The output of the BPF is amplified to generate the main channel output signal  $d(t)$ . The auxiliary channel output  $N_r(t)$  is generated similarly by a duplicate set of hardware. The signal simulator can generate identical signals in the main and auxiliary channels as well as time and/or phased delayed versions of the main channel signal in the auxiliary channel.

**3.4 Experimental Results.** The closed loop system response was tested with inputs consisting of both CW monotone signals and wideband signals. Tests were performed, with both an applied DC field and an applied AC square wave field across the BSO crystal, to measure the system's cancellation performance. Cancellation speed (or system response time measurements) were only measured with an applied DC field. The signal simulator hardware was used to generate the monotone CW inputs as well as wideband inputs with bandwidths of 100 kHz, 200 kHz, and 500 kHz centered at 40 MHz.

**3.4.1 Cancellation with Applied DC Field.** Shown in Fig. 9 is the cancellation of a 40 MHz monotone signal.

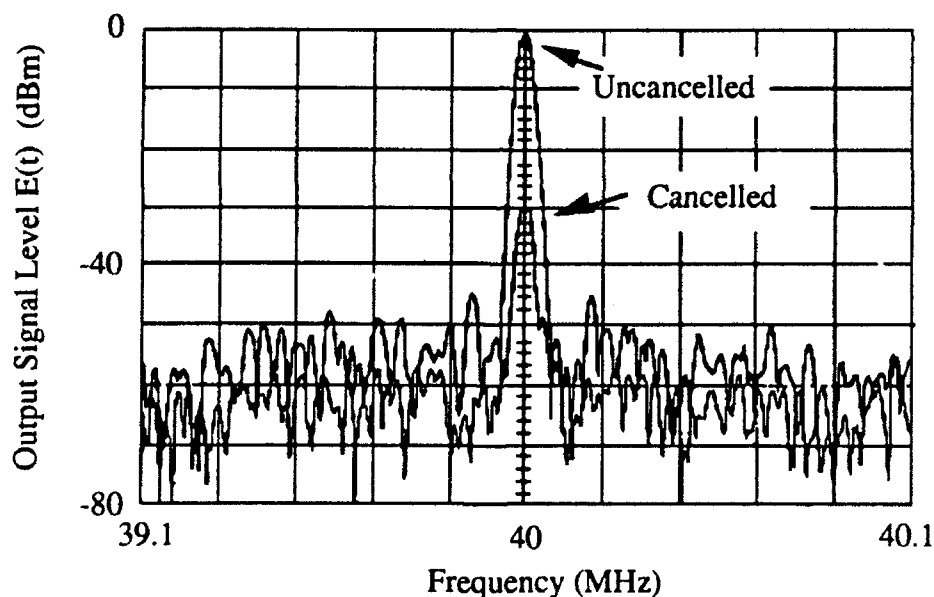
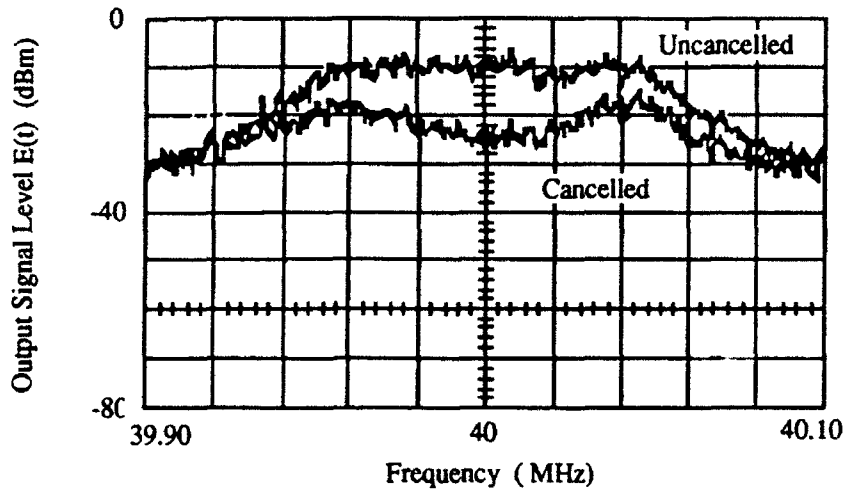
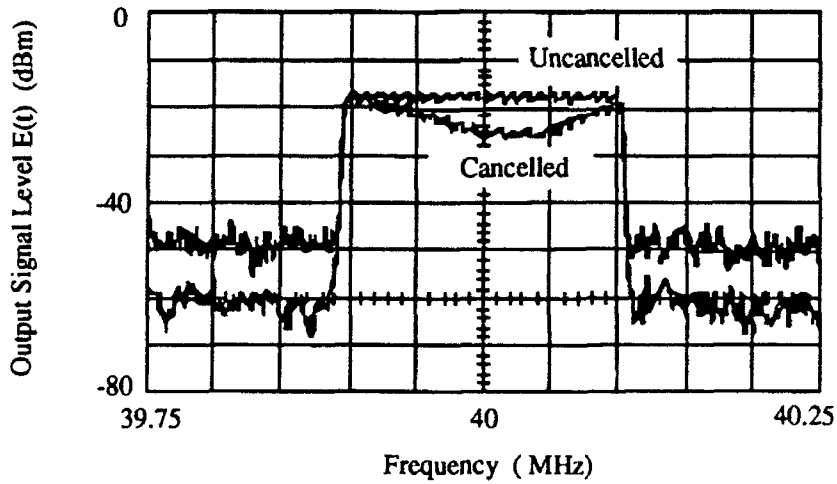


Fig. 9. Cancellation of 40-MHz monotone CW signal with applied DC field.

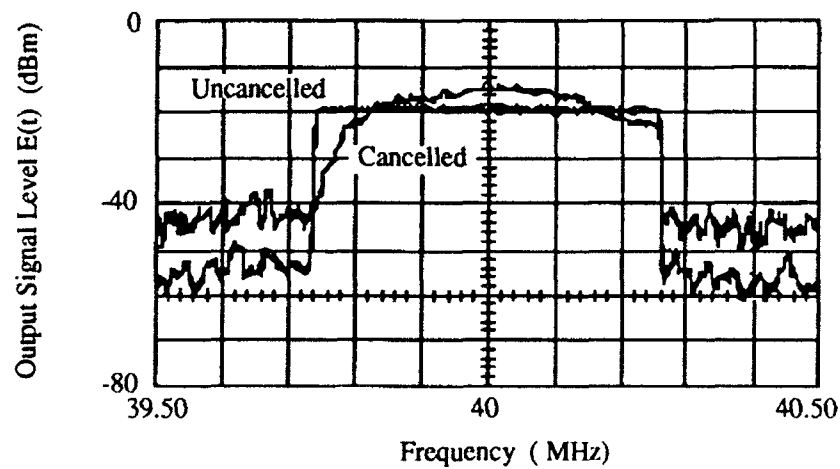
A DC field of 8 kV was used primarily to keep from damaging the crystal and still provide a high level of diffraction. The system is able to provide 29 dB of cancellation. Further amplification tends to raise the noise floor without achieving substantial improvements in cancellation performance. We demonstrated 25-dB cancellation of monotone CW signals spaced at 2 MHz over a 8 MHz band between 36 and 44 MHz.<sup>11</sup> The wideband cancellation results are shown in Fig. 10. As can be seen the cancellation performance falls off rapidly with increasing bandwidth.



a) 100-kHz bandwidth



b) 200-kHz bandwidth



c) 500-kHz bandwidth

Fig. 10. Cancellation of wideband noise signals a) 100 , b) 200, c) 500 KHz centered at 40 MHz with applied DC field.

Cancellation performance beyond 500 kHz was inconclusive. Applied fields approaching 10 kV allowed us to obtain cancellation approaching 40 dB for a 40-MHz monotone signal. However, the large applied fields are more likely to damage the crystal with extended use. The results obtained with the DC field are examined in more detail in Section 4.

**3.4.2 Cancellation with Applied AC Field.** An applied square wave AC field was also used to determine if the diffraction efficiency of the crystal could be enhanced to improve cancellation results. It was also believed the output would be more stable using the AC field because the generation and recombination of the free electrons and traps are effectively smoothed by an AC field of an appropriate frequency. Various field strengths and frequencies were used to determine optimum operating conditions for the system in closed loop operation. Large phase fluctuations were noticed in the systems output signal, especially for slight variations in the polarization of the input light. By fine tuning the quarter waveplate in the read beam before the BSO crystal (see Fig. 8) the phase fluctuations could be reduced. The optimum applied voltage was around 4 kV peak to peak. The optimum square wave frequency was 1.6 kHz which is closer to the upper limit of the amplification units rise time. Shown in Fig. 1 is the cancellation of a 40 MHz monotone signal, with approximately 24 dB of cancellation.

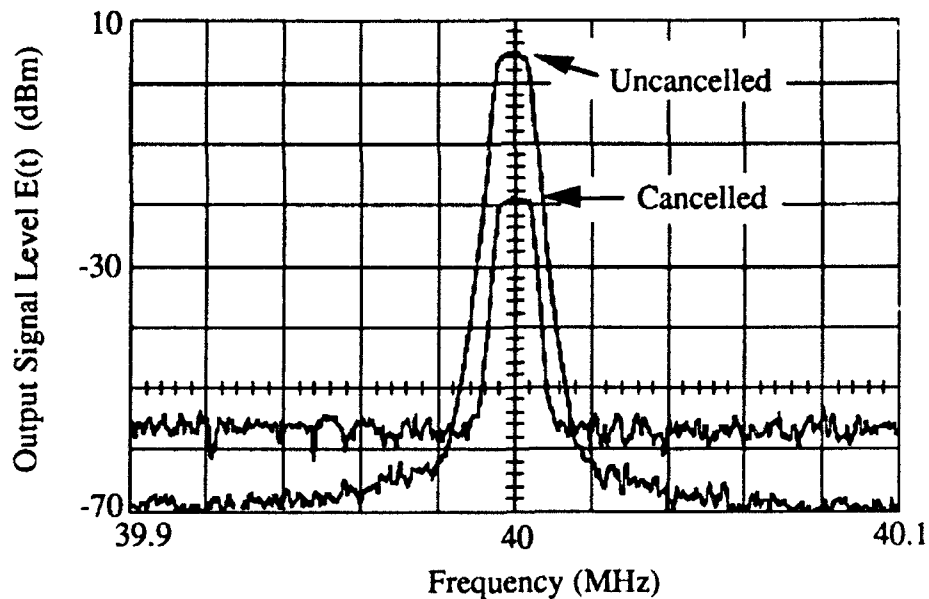
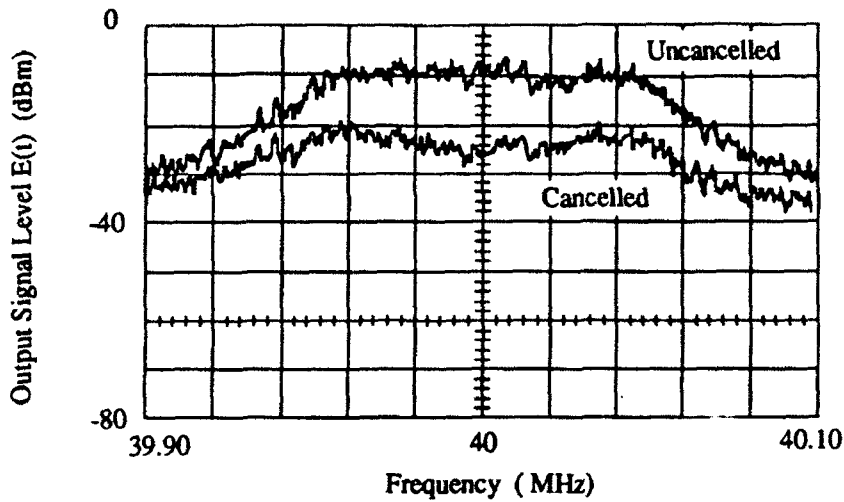
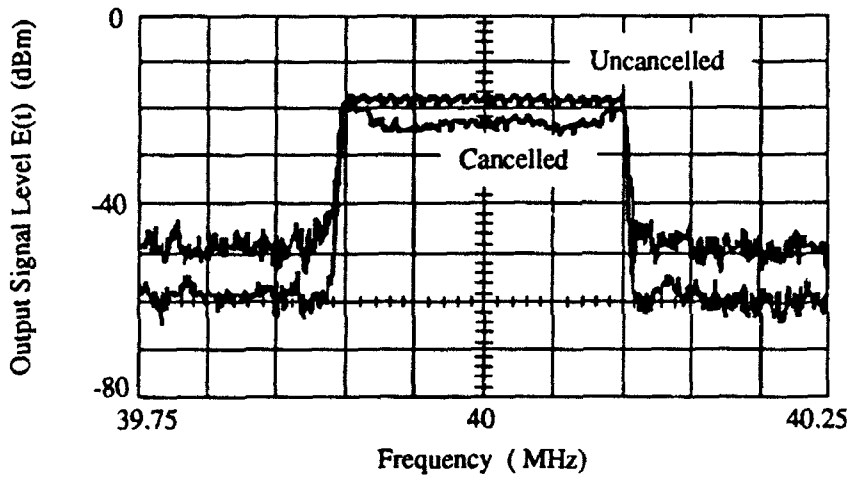


Fig. 11. Cancellation of 40-MHz monotone CW signal with AC applied field.

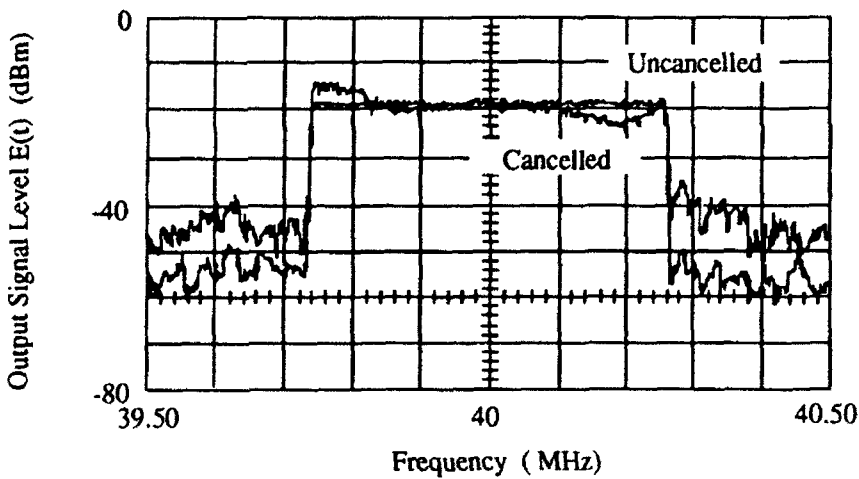
In this case the system did not cancel as close to the noise floor, however, more amplification only raised the noise floor but did not improve cancellation. The wideband cancellation using the applied AC field are shown in Fig. 12. As can be seen the cancellation performance falls off rapidly with increasing bandwidth. Cancellation performance beyond 500 kHz was inconclusive.



a) 100-kHz bandwidth



b) 200-kHz bandwidth



c) 500-kHz bandwidth

Fig. 12. Cancellation of wideband noise signals a) 100 , b) 200, c) 500 KHz centered at 40 MHz with applied AC field.

**3.4.3 Cancellation speed.** Finally cancellation speed was measured. The system was operated in the closed loop mode with a shutter placed in the focal plane of the imaging system of the time integrating correlator (see Fig. 7). The shutter acted as a switch controlling the writing of the correlation grating on the BSO crystal. A high speed oscilloscope was used to measure the output of the system before and after the shutter was opened. The measured cancellation speed is shown in Fig. 13. The signal is cancelled in approximately 1.2 msec as shown in this plot. The oscilloscope was triggered off the same signal used to open the shutter in the set-up. We also measured the speed at which the shutter opened to make sure it wasn't limiting system performance. The shutter speed was approximately 0.5 msec. Therefore, it is possible the system might be operating a little faster than shown.

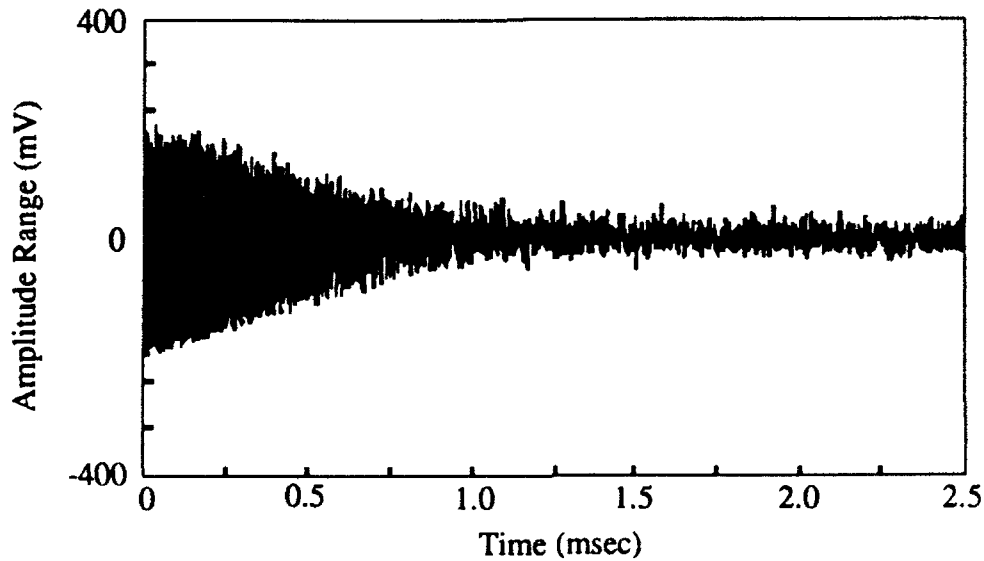


Fig. 13. Cancellation of a 40 MHz monotone signal with respect to time.

#### 4. Discussion

The concept of loop gain was presented by Montgomery<sup>3</sup> to describe the behavior of the closed loop adaptive architecture. This approach to evaluating system performance provides a good first approximation for describing the effects of increasing the signal bandwidth on system cancellation performance. The general premise of evaluating the open loop gain is that each component in the loop either contributes gain or loss to the overall system. The maximum cancellation performance is then related to the amount of gain the feedback loop provides for canceling the input noise signal  $N_o(t)$  from  $d(t)$ . Fig. 14 shows the components of the mod-AOAP which contribute gain or loss to the closed loop system. If something adds loss to the system then the overall loop gain will decrease and the cancellation performance will also decrease. Based on this intuitive approach, the relationship between bandwidth and the diffraction efficiency of the PRC is examined to determine the effect on the adaptive system's open loop gain.



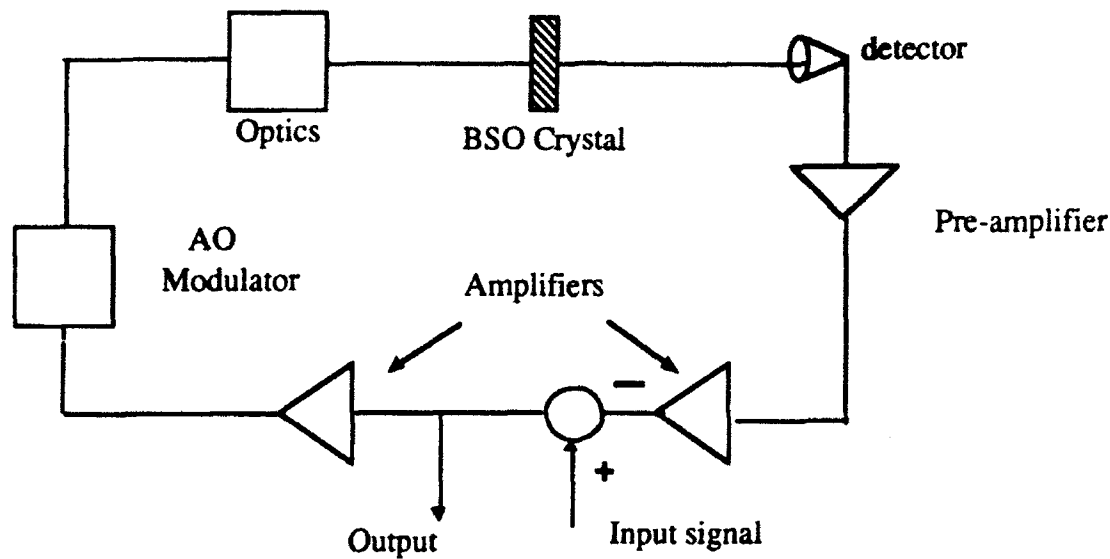


Fig. 14. Block diagram of closed loop system gain components.

**4.1 Predicted Cancellation.** A computer model was developed to determine the influence of increasing bandwidth on the correlation result, which in turn affects the diffraction efficiency of the photorefractive crystal. The model is intended to provide only a general understanding of wideband correlation and the resulting PRC diffraction efficiency. The assumption is that all variables except the input signal's bandwidth are kept constant in the experimental setup used to perform narrowband and wideband measurements. The bandwidth in the model is increased by representing the wideband signals as a sum of individual signals at 10-kHz spacing, which is consistent with our signal simulator. The computer simulation (see Appendix) was written in MATLAB and developed using References 3,8,12,13, and 14.

The model uses the input  $N_r(t)$  to determine the output of AO-2 and uses the output of AO-2 to determine the grating intensity on the PRC. There are limits to the diffraction efficiency of AO-2 caused by a required spur free dynamic range (SFDR) to reduce the effects of intermodulation products caused by the wideband input.<sup>8</sup> The amplitude of the acoustic waves in AO-2 caused by each frequency is summed to obtain the composite signal in the cell. The composite wave is in the form of a traveling spatial wave. The waveform is multiplied by the sum of waves at a point in time to obtain an amplitude for this discrete point in time. A "frozen" waveform is obtained by doing this repeatedly across the AO cell time aperture. The resulting acoustic amplitude wave is squared to obtain the diffracted intensity pattern collected at the PRC. The envelope of the photorefractive grating is used to find the modulation index  $m$  across the photorefractive crystal. The point by point modulation index is combined with the intensity pattern across the PRC to determine the point by point diffraction efficiency of the PRC. The total diffraction efficiency of the PRC is found by summing the point by point diffraction efficiencies. The model's predicted diffraction efficiency versus input signal bandwidth is plotted in Fig. 15.

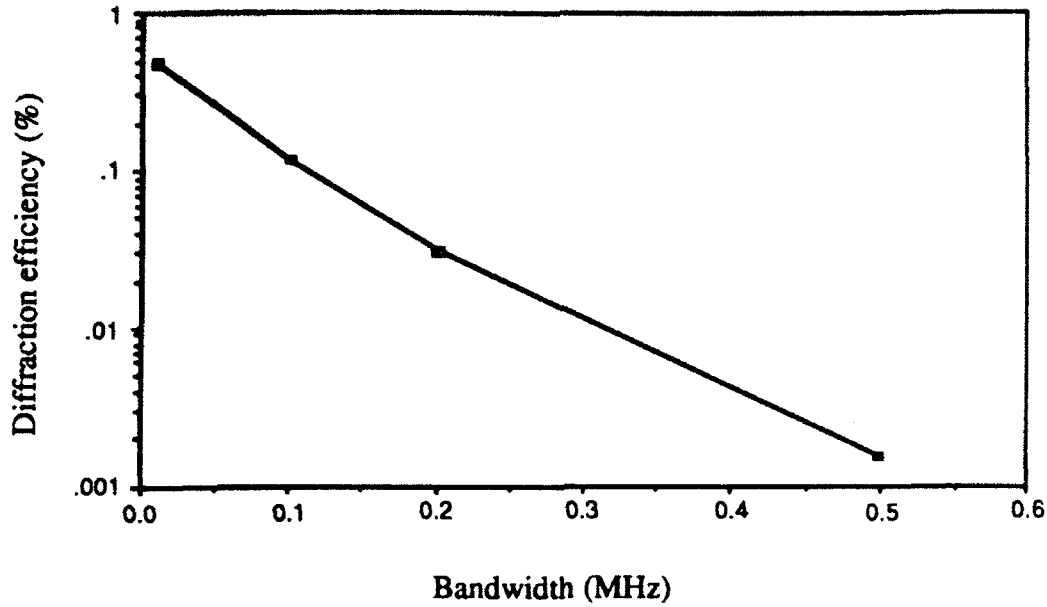


Fig. 15. Predicted diffraction efficiency versus noise signal bandwidth.

Returning to the open loop gain model, the cancellation performance will be degraded in direct proportion to the diffraction efficiency loss. The normalized system's gain versus bandwidth is plotted in Fig. 16 for the computed and experimental results.

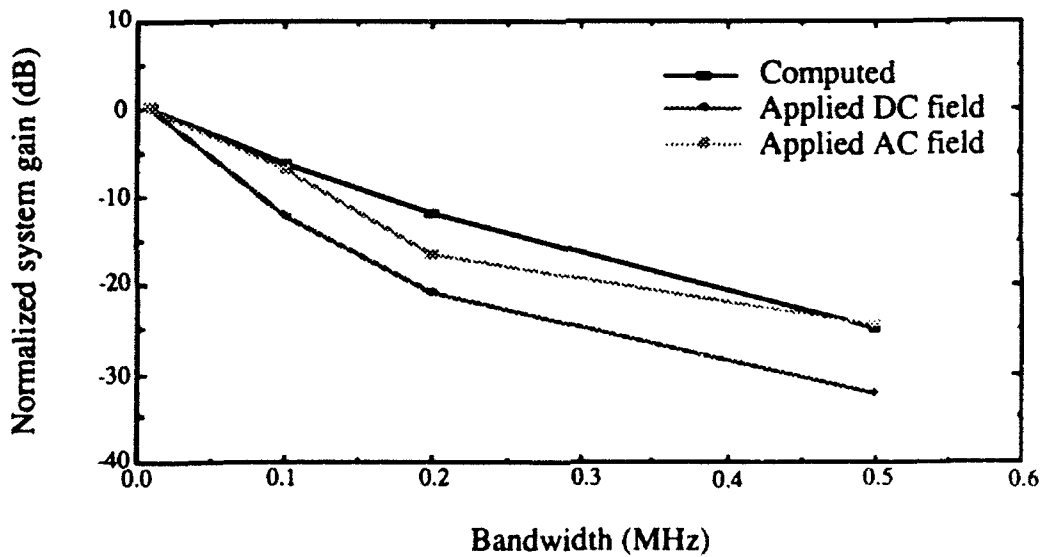


Fig. 16. Normalized system gain with respect to noise signal bandwidth. Results are normalized to 0 dB for a monotone CW input signal.

The computed results are normalized with respect to the diffraction efficiency of a monotone CW input signal. The DC experimental results are normalized with respect to the 29 dB of cancellation obtained for a 40-MHz monotone signal as shown in Fig. 9. The AC field experimental results are normalized with respect to the 24 dB of cancellation for a 40-MHz monotone signal as shown in Fig. 11. The computer model helps explain the decrease in cancellation performance with increasing noise bandwidth demonstrated in Fig. 17. The AC field results more closely match the predicted performance. However, our DC field cancellation performance falls off more rapidly than explained by our model. A more in-depth study of the optical activity of BSO is necessary to accurately model the devices performance for wideband cancellation. Discussions with George Brost and John Hong indicate the instabilities are greater when only applying a DC field. Other system properties which need to be examined to determine their effects on system cancellation include vibration, air currents, non-uniform optical magnification, non-linearities in the electronics, and the detector noise.

**4.2 Comparison of AOAP and mod-AOAP.** The use of the BSO photorefractive crystal in the adaptive processor demonstrated approximately the same cancellation properties as the LCLV and exhibited a faster response time. Neither approach exhibits adequate cancellation for wideband jamming signals which may be present in a radar system's IF. Our computer model predicts cancellation performance will deteriorate with increasing bandwidth. Therefore, an integrator/spatial light modulator which provides higher efficiency and larger dynamic range is necessary.

## **5. Conclusions and Recommendations**

**5.1 Conclusions.** The driving application for the adaptive optical processor presented in this report is to null radar jamming. We have presented results demonstrating the performance of an optical implementation of the LMS algorithm using a photorefractive crystal as the time integrating device. While the system provides a time response on the order of 1 msec, our data suggests that jammer cancellation performance is highly dependent on the jamming noise signal bandwidth. For monotone CW jammers, the system is able to provide greater than 25-dB cancellation over an 8-MHz band. For wideband noise signals (>100 kHz) our analysis shows that cancellation performance falls off rapidly with increasing bandwidth. We have modeled the wideband signal's amplitude effects on the grating formed in the photorefractive crystal. The model provides a first approximation which helps explain some of the degraded performance, however, other effects must still be explored.

**5.2 Recommendations.** The loop gain model provides a simplified approach for analyzing those components which affect overall cancellation performance. Further studies of photorefractive crystals are necessary to determine if the diffraction efficiency can be increased so that overall loop gain is improved. Alternative means of performing the integration/spatial light modulation also need to be examined, to see if devices with comparable speed and better efficiency can be found. Along with examining other lossy and noisy components of the system (the acousto-optics, lenses, and the detector), a means of controlling electronic amplification during cancellation is necessary to increase closed loop gain as the input signal level decreases.

## References

1. Penn, W.A. "Acousto-optic adaptive processor (AOAP) - Phase II," Final Technical Report, RADC-TR-86-188, November 1986.
2. Wasiewicz, R., R.M. Iodice, W.A. Penn, D.B. Friedman, "Acousto-optic adaptive processor (AOAP) enhancements," Final Technical Report, RL-TR-92-13, February 1992.
3. Montgomery, R.M., M.R. Lange, "Photorefractive adaptive filter structure with 40-dB interference rejection," Applied Optics, Vol.30, No. 20, 2844 - 2849, 1991.
4. Vachss, F., J.H. Hong, C.W. Keefer, J.E. Malowicki, "Operation of an adaptive processor using a photorefractive parallel integrator," Proc. SPIE, Vol. 1703, Optoelectronic Signal Processing for Phased Array Antennas III, 1992.
5. Montgomery, R.M., W.R. Beaudet, M.R. Lange, "Photorefractive adaptive sidelobe canceler for phased array antennas," Proc. SPIE, Vol. 1703, Optoelectronic Signal Processing for Phased Array Antennas III, 1992.
6. Wasiewicz, R., D.B. Friedman, "Penn-Dickey acousto-optic adaptive processor (AOAP) development," Proc. SPIE, Vol. 1703, Optoelectronic Signal Processing for Phased Array Antennas III, 1992.
7. Widrow, B., P. Mantey, L. Griffiths, B. Goode, "Adaptive antenna systems," Proc. of the IEEE, Vol. 25, 2143-2149, 1967.
8. VanderLugt, A., Optical Signal Processing, John Wiley & Sons, New York, 1992.
9. Grinberg J., A. Jacobsen, W.P. Bleha, L. Miller, L. Fraas, D. Boswell, G. Myer, "A new real-time non-coherent to coherent light image converter the hybrid field effect liquid crystal light valve," Optical Engineering, Vol. 14, 217-225, 1975.
10. Ruterbusch, P.H., "Hughes liquid crystal light valve tests," GE In-House Tech Memo, July 1992.

11. Keefer, C.W., J.E. Malowicki, P.M. Payson, "Wideband operation of a photorefractive based adaptive processor," Proc. SPIE, Vol. 1790, Analog Photonics, 1992.
12. Stepanov, S.I., M. P. Petrov, "Nonstationary holographic recording for efficient amplification and phase conjugation," in Photorefractive Materials and Their Applications I, P. Gunter and J.-P. Huignard, eds., Vol. 61 of Topics in Applied Physics, Springer-Verlag, Berlin, 263-289, 1988.
13. Montgomery, R.M., "Acousto-optic/photorefractive processor for adaptive antenna arrays," Proc. SPIE, Vol. 1217, Optoelectronic Signal Processing for Phased Array Antennas II, 1990.
14. Leckavich, J., "Basics of acousto-optic devices," Lasers and Applications, 59-64, April 1986.

## Appendix

### Diffraction efficiency simulation program

```

% Model of time integrating correlator Program name"prgr"
% July 21 1992

% Vanderlugt pg358 Signal Compression
% When many signals share the same diffraction efficiency,
% the acousto-optic cell becomes source depleted

clear,clg,hold off
cstart=clock;          % To start program duration clock
v=3900;                % Acoustic wave velocity m/sec
fc=40e6;BW=.1e6;step=.01e6; % Center Frequency, Bandwidth, Frequency Interval
fs=fc-BW/2;res=2.5e2/fc;Q=BW/step; % start freq., Q = number of frequencies
prgrat=0;

%-----Diffraction eff in AO for good Dynamic Range-----

SFDR=5e4;              % Spur Free Dynamic Range !Set higher for more freq.
                      % This was held constant for all cases
C=1-(2*(2*Q-1)/sqrt(SFDR)); % Compression of signal in AO cell
CC=abs(10*log10(C));   % Compression in db
nf=3*(1-C)/(2*Q-1);   % The diffraction eff. per unit frequency
ne=nf*(1-nf*(2*Q-1)/3) % The effective diffraction eff. per frequency
if C > (ne/nf + .00001), % Check to see if equations in valid range
    invalid = 1      % If not, => invalid
end
check=36/nf^2;        % Check to see if equations in valid range

%-----

p=0;f=fs;

```

```

fcar=200e6; % Carrier frequency of point
modulator
stop=100e-4; % 1/2 AO cell size in meters
x=(-stop:1e-5:stop); % AO cell size in meters
length(x)
phase=0;T=1e-3; % Integration time T
% phase=2*pi*rand(1,BW/step); % Random phase variable
strobe=0;tstop=5*fs*T; % This no. would allow integration to 1ms but not done
pow=40;amp=pow/Q; % Amplitude of signals from total amplitude level 40

%-----For Loop-----

con=2*pi;posit=-T/2-x/v;
for ii = 1:11:720*11, %For time integration in steps of 5.5069e-08sec
    % Should go to tstop=1ms, but only 720*5.5069e-08sec
    t= ii/(5*fs);
    countdown=720-ii % To monitor program progress
    p=0;si=0;ssenv=0;senv=0;xenv=0;
    multit=0; strob=0;
    for i=1:(BW/step)+1, % Strobing
        strob=cos(con*f*t)+strob; % Sum of wave amplitudes to point modulator
        p=amp*cos(con*f*(t+posit))+p; % Sum of acoustic waves in 2nd cell
        f=fs+i*step;
    end
    p=ne*p*strob; % It makes a difference to multiply here or in for loop
    % "p" is the frozen wave pattern

%-----Envelope of Acoustic wave-----

L=length(p);c=1,num=2;a=1;max=0;
for a=2:L-1, % Finds max points of the wave
    if p(a-1)<p(a),
        if p(a)>p(a+1),
            even=rem(num,2);num=num+1;

```

```

    if even == 0,          % Takes every other point to reduce no.
        ssend(c)=p(a);xenv(c)=x(a);c=c+1;
    end
end
end
end
si=spline(xenv,ssenv,x); % Fits a curve to the peak points => envelope

%----- Diffraction eff and Pr-----

% From John Lekavich's paper
lam=514e-9;pp=0;A=5;M=9e-15;P=si.^2;
phase=(pi/lam)*(2*A*M.*P).^5;
n=(sin(phase./2)).^2;
prgrat = n.*(p).^2 + prgrat; % Photorefractive INTENSITY pattern weighted
                             % by AO cell diffraction eff.

%-----

fs=fc-BW/2;f=fs;          % reset for next time step
end

%-----End of For Loop-----

clg,hold off             % Plots
subplot(211),plot(x,p,'r'),grid,hold on % Plot waveform of 2nd AO cell
fend=fc+BW/2;
title(['AO cell ',num2str(fs),' to ',num2str(fend),' in ',num2str(step),' Steps'])
xlabel('Position in meters')
ylabel('Amplitude')

subplot(211),plot(xenv,ssenv,'o')
subplot(211),plot(x,si)

```



```
save grating.dat prgrat /ascii % Save data
```

```
%-----Envelope of Photorefractive Grating-----
```

```
skip = 0;
if skip == 0,
min=0;max=0;c=1;cc=1;
[m,LL]=size(prgrat);
for j=2:(LL-1), % Finds max and min points of the wave
if prgrat(j-1)<prgrat(j),
if prgrat(j)>prgrat(j+1),
max(cc)=prgrat(j);maxx(cc)=x(j);cc=cc+1;
end
end
if prgrat(j-1)>prgrat(j),
if prgrat(j) <prgrat(j+1),
min(c)=prgrat(j);minx(c)=x(j);c=c+1;
end
end
end
prmax=spline(maxx,max,x); % Fits a curve to the max points => upper envelope
prmin=spline(minx,min,x); % Fits a curve to the min points => lower envelope
end
```

```
%-----
```

```
% More Plots
```

```
hold off,subplot(212),plot(x/2,prgrat),grid,hold on
title('PhotoRefractive Grating')
xlabel('Position in meters')
ylabel('Amplitude')
subplot(212),plot(maxx/2,max,'o')
subplot(212),plot(minx/2,min,'x')
```

```

subplot(212),plot(x/2,prmax,'g')
subplot(212),plot(x/2,prmin,'g')

% effect on the modulation index
% eq. for m from "Optimal properties of photorefractive materials for optical
% data processing", Optical Engineering, Vol. 22, eq 6

%-----Photorefractive Diffraction Eff.-----

[sizem,sizei]=size(si);
I1=prmin +5000;I2=prmax; % Min wave biased up so that m won't go past 1
m=2*(I1.*I2).^5./(I1 + I2); % Modulation index between upper and lower waves
[mm,kk]=size(m);
    % Diffraction eff. according to George -> Huignard
    % Values taken from Fred Vachss-Photorefractive >
    % Transfer Function
k=2*pi/50e-6; % Grating spatial frequency
T=290; % Temp in degrees Kelvin
Ed=.026 *k *T/300; % Eff electric field due to charge diffusion
Eq=7e11/k; % Maximum value of Esc, charge saturation limited
Eo=7e3; % Applied electric field
    % Space charge field, below
Esc=Eq*((Eo^2 + Ed^2)/(Eo^2 + (Ed + Eq)^2))^5;
dE= m(50:kk-50)*Esc;
Idiff= (sin(.5*pi*8.2e-11*dE*1e-2/(514e-9))).^2; % Photorefractive diffraction
xx=x/2;

hold off % Plots
subplot(111),plot(xx(50:kk-50),Idiff),grid
title('Diffracted Intensity')
xlabel('Position')
ylabel('Relative Amplitude')
total=sum(Idiff)/Q; % Total amount of light diffracted per frequency
etime(clock,cstart)

```

**MISSION  
OF  
ROME LABORATORY**

*Rome Laboratory plans and executes an interdisciplinary program in research, development, test, and technology transition in support of Air Force Command, Control, Communications and Intelligence (C<sup>3</sup>I) activities for all Air Force platforms. It also executes selected acquisition programs in several areas of expertise. Technical and engineering support within areas of competence is provided to ESD Program Offices (POs) and other ESD elements to perform effective acquisition of C<sup>3</sup>I systems. In addition, Rome Laboratory's technology supports other AFSC Product Divisions, the Air Force user community, and other DOD and non-DOD agencies. Rome Laboratory maintains technical competence and research programs in areas including, but not limited to, communications, command and control, battle management, intelligence information processing, computational sciences and software producibility, wide area surveillance/sensors, signal processing, solid state sciences, photonics, electromagnetic technology, superconductivity, and electronic reliability/maintainability and testability.*